A Study on the Behavior of UHPC Sheet Piles

Tuan Nghia Hoang
Department of Steel and Timber Structures, Hanoi University of Civil Engineering, Hanoi, Vietnam
nghiaht@huce.edu.vn

Cong Thang Nguyen
Department of Building Materials, Hanoi University of Civil Engineering, Hanoi, Vietnam
thangnc@huce.edu.vn

Viet Hung Cu
Department of Bridges and Roads, Hanoi University of Civil Engineering, Hanoi, Vietnam
hungcv@huce.edu.vn (corresponding author)

Keun-Hyeok Yang
Department of Architectural Engineering, Kyonggi University, Kyonggi-do, South Korea
yangkh@kgu.ac.kr

Van Tuan Nguyen
Department of Building Materials, Hanoi University of Civil Engineering, Hanoi, Vietnam
tuannv@huce.edu.vn

Received: 9 June 2025 | Revised: 10 September 2025 | Accepted: 19 September 2025

 DOI: https://doi.org/10.48084/etasr.12606

ABSTRACT

Steel and Reinforced Concrete (RC) sheet piles have been widely used in infrastructure applications. However, they are associated with significant drawbacks, including their high cost and susceptibility to corrosion in steel piles. They are also heavy, difficult to handle, and less durable in RC piles. This study proposes a novel approach using Ultra-High-Performance Concrete (UHPC) as an innovative alternative to address these limitations. UHPC was successfully developed using locally available materials, incorporating 2% steel fiber and achieving compressive and flexural strengths exceeding 120 MPa and 12 MPa, respectively. A new sheet pile cross-section was designed using the Wavy-type (SW), in accordance with Japanese standard JIS A5373:2004, and reinforced with normal steel bars (CB400V). The structural performance was evaluated through both theoretical calculations and experimental testing, covering the elastic, first cracking, and ultimate load stages. The findings demonstrate the feasibility and advantages of UHPC sheet piles, offering a lightweight, highly durable, and corrosion-resistant solution that addresses the key shortcomings of conventional materials. This research contributes to the advancement of sustainable and resilient construction practices, particularly in aggressive environments.

Keywords-ultra-high-performance concrete; sheet pile; flexural behavior; load-deflection behavior; first crack; reinforcements

I. INTRODUCTION

Erosion control in civil constructions, transportation infrastructure, wharves, and irrigation works is a critical issue for ensuring the safety and stability of these facilities. Traditionally, the common solutions include RC piles, retaining walls, and various shore protection systems such as foundation pits. These techniques, however, often require a large number of piles, take a long time to complete, and are expensive, reducing the return on investment. To address these drawbacks, steel Larsen sheet piles or prestressed RC sheet piles are used globally, including in Vietnam. The steel Larsen sheet piles are interlocking sheet members that form closed retaining walls, primarily designed to prevent water and soil intrusion. Larssen sheet piles were developed in 1906 by Trygve Larssen [1-3], with their first application in 1908 in the US in the Black Rock Harbor project with outstanding results. Steel sheet piles remain widely used today across various applications, including road works and traffic tunnels (Larsen sheet piles are used to stabilize slopes and embankments) [4]. In civil works, steel sheet piles serve as tunnel walls in multi-story buildings and underground parking structures, replacing conventional RC walls. These sheet piles are also employed as retaining walls to prevent soil and water ingress during excavation works, etc.

Steel Larsen sheet piles are extensively used for temporary and permanent structures, but are not economically viable for projects that need to keep sheet piles permanently due to cost and corrosion in aggressive environments. These limitations have driven the need for alternative solutions, particularly in projects requiring long-term durability and cost efficiency. In response, the concrete sheet piles have been developed to reduce material costs and mitigate corrosion risks. Conventional RC sheet piles typically require large cross-sectional thicknesses (10–15 cm) to achieve the necessary strength and durability. This results in increased weight, logistical challenges during transportation and installation, leading to higher construction costs, especially in confined construction spaces.

The inherent drawbacks of both steel and conventional concrete sheet piles have motivated the exploration of a new generation of hybrid piles, fabricated from UHPC. UHPC has been developed globally since the 1990s [5, 6] and exhibits outstanding properties, such as very high compressive strength (generally exceeding 120 MPa) [7, 8], high flexural strength, excellent impact and fatigue resistance, and remarkable durability under aggressive environmental conditions. These superior characteristics have expanded UHPC applications to encompass more durable, lightweight, and eco-friendly structural solutions.

Significant progress has been made in understanding UHPC, with design guidelines developed in countries such as France, USA, and Germany. Successful projects across Canada, Europe, Asia, and USA have confirmed its superior durability, cost-effectiveness, and long-term performance [6, 9, 10]. UHPC has also gained attention for transportation infrastructure, especially in pile foundations and sheet pile systems [11-13].

In Vietnam, research on UHPC has progressed, with notable examples including [14, 15]. Initial applications and ongoing studies focused on optimizing UHPC properties with the use of mineral admixtures [16-19]. For instance, authors in [20] proposed a novel approach utilizing UHPC sheet pile walls combined with gabion groynes. This innovative solution was implemented at Rung Duong Resort in Ba Ria–Vung Tau and successfully improved the coastal protection, advanced the shoreline, and facilitated sandy beach formation. Furthermore, UHPC has been increasingly adopted in Vietnam for thin-walled, impact-resistant structures [21-23], underscoring its versatility and performance advantages. The exceptional physical and mechanical properties of UHPC not only offer enhanced durability and reduced environmental impact, but also enable more efficient structural design. For example, UHPC reduces the cross-sectional area of load-bearing elements, which decreases self-weight, reduces foundation loads, simplifies construction processes, and alleviates prestressing requirements. These benefits collectively highlight UHPC as a promising material for the next generation of sheet pile applications in challenging environments.

The present study investigates the potential of using UHPC for the production of sheet piles, emphasizing its ability to reduce cross-sectional thickness while achieving technical performance comparable to steel Larsen sheet piles. At the same time, it overcomes the drawbacks of traditional precast concrete sheet piles, particularly by facilitating easier transportation and installation. Moreover, UHPC sheet piles, when reinforced with conventional steel rebars, present a cost-effective and corrosion-resistant alternative to the commonly used steel Larssen sheet piles. Therefore, the research, fabrication, and evaluation of the load-bearing capacity of UHPC sheet piles reinforced with standard steel reinforcement possess both scientific importance and practical relevance, contributing to the advancement of durable and cost-effective solutions for infrastructure in challenging conditions.

II. MATERIALS AND METHODS

A. Materials

The materials employed include quartz sand (S) with a mean particle size of 300 μm and Portland cement PC40 in accordance with the technical requirements of Vietnamese standards TCVN 2682: 2009. An undensified Silica Fume (SF) was used with a mean particle size of 0.15 μm and a bulk density of 250 kg/m^3. The chemical composition and properties of the cementitious materials determined using X-ray Fluorescence (XRF) are shown in Tables I and II, respectively. The particle size distribution of sand and cementitious materials is depicted in Figure 1. Superplasticizer (SP) with a solid content of 30% by mass was utilized to achieve the workability of UHPC mixtures from 150 to 200 mm to ensure uniformity and consistency. The steel fiber used is OL 13/0.2, with a length of 13 mm, a diameter of 0.2 mm, and a tensile strength exceeding 2500 MPa.

TABLE I. CHEMICAL COMPOSITIONS OF CEMENTITIOUS MATERIALS

Materials	Cement, wt.%	SF, wt.%
SiO_2	20.60	92.30
Fe_2O_3	5.130	1.910
Al_2O_3	3.560	0.860
CaO	63.26	0.320
MgO	3.070	0.850
Na_2O	0.240	0.380
K_2O	0.250	1.220
SO_3	-	0.300
L.O.I	1.860	1.680

TABLE II. PROPERTIES OF CEMENTITIOUS MATERIALS

Property		Unit	Cement	SF
Fineness (Blaine)		cm^2/g	3870	-
Mean particle size		μm	11.40	0.150
Specific gravity			3.150	2.200
Pozzolanic reactivity index		%	-	113.5
Compressive strength	After 3 days	MPa	29.80	-
	After 28 days	MPa	52.20	-

B. UHPC Compositions

Based on the particle size distribution of these materials determined by laser diffraction, as exhibited in Figure 1, the maximum packing density of the granular composition was calculated deploying the method proposed in [24, 25], where the compaction coefficient of the granular composition was 12.5 as proposed in [21]. For the mixed system of sand - cement - SF, SF replaced cement by 0-40% by weight. In this

case, the binder can be considered a combination of cement and SF. Therefore, the particle composition is considered a two-component system consisting of sand and binder. The relationship between the compaction of the mixture and the ratio of the component materials is illustrated in Figure 2. From these calculations, the optimal amount was determined to have a sand-to-(sand + binder) ratio of 0.50 by weight.

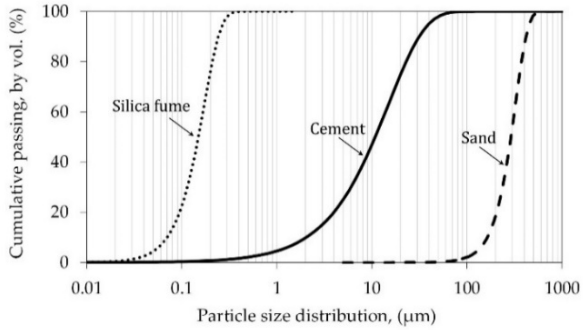

Fig. 1. Particle size distribution of materials used in this study.

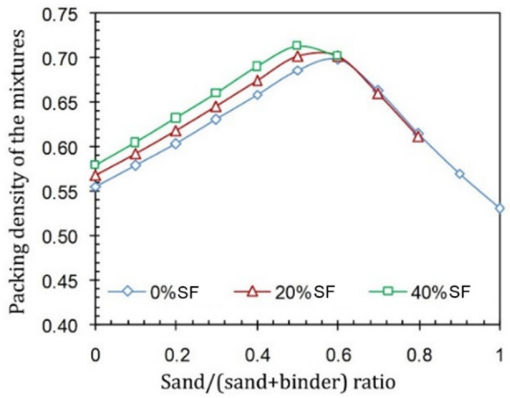

Fig. 2. Packing density of the granular mixture of sand–cement–SF.

The composition of the UHPC mixture to produce sheet piles is given in Table III.

TABLE III. MIX COMPOSITION OF THE UHPC MIXTURE

w/b, by weight	0.16
s/b, by weight	1
SF, wt.% by binder	20
SP, wt.% by binder	1.30
Sand, kg/m^3	1090
Cement, kg/m^3	875
SF, kg/m^3	218
SP, g/m^3	47.3
W, kg/m^3	154
Fiber, kg/m^3	157

C. Mixing Process and Property Testing of UHPC

The materials were measured and mixed following the procedure presented in Figure 3. Mixing was followed by flowability adjustment, and then the samples were cast to evaluate the compressive strength, flexural strength, and elastic modulus. The mechanical properties of UHPC were tested at the age of 28 days. The compressive strength and elastic modulus of UHPC were determined using cylindrical samples of 100 mm × 200 mm size, as portrayed in Figure 4(a). The flexural strength of UHPC was determined on prism samples of 100 mm × 100 mm × 400 mm size, as evidenced in Figure 4(b). The experimental results of UHPC are outlined in Table IV. The properties of UHPC obtained were used in the design and production of sheet piles.

TABLE IV. MECHANICAL PROPERTIES OF UHPC

Properties	Units	Value	Test method
Compressive strength (R_{bn})	MPa	120	ASTM C39M [22]
Flexural strength (R_{bt})	MPa	12	ASTM C1609M [23]
Modulus elastic (E)	GPa	48	ASTM C469M [24]

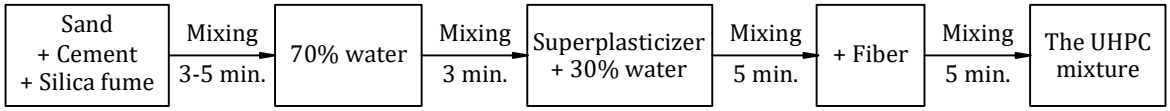

Fig. 3. Mixing process of the UHPC mixture.

(a) (b)

Fig. 4. Testing of UHPC: (a) compression test, (b) flexural strength test.

III. DESIGN AND OPTIMIZATION

A. Design of UHPC Sheet Pile

1) Materials

Based on the obtained results, UHPC was chosen as the material for the pile, with its parameters shown in Table IV. The reinforcement used is CB400V type, in accordance with TCVN 5574-2018, with a calculated tensile strength of R_s = 350 MPa, E_s = 210,000 MPa, and elongation of 14 %.

2) Section

The selection of the sheet pile model in this study was based on the Japanese Industrial Standard (JIS-A5373, 2004), which classifies various sheet pile types, including the Wavy

type (SW) cross-section. According to the specifications of the proposed guidelines (Section 3.1) of JIS-A5373 (2004), as provided in Table IV, the standard SW sheet pile dimensions are considerably large, particularly the wall thickness, which typically ranges from 60 mm to 120 mm. Such a large thickness results in heavy structural components, leading to challenges in transportation, handling, and installation. Furthermore, the large wall thickness increases soil resistance during driving, thereby complicating the pile installation in the field.

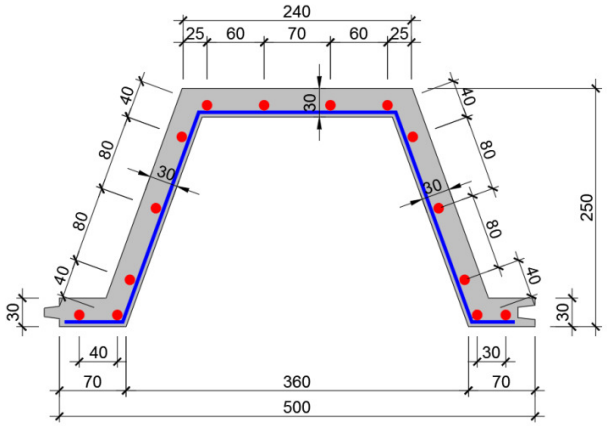

Fig. 5. Arrangement 14ϕ12 type CB400V bars for UHPC sheet piles.

To address these challenges, the current study proposes the use of UHPC, which, due to its superior compressive strength, allows for a significant reduction in wall thickness without compromising the structural performance. By adopting UHPC, the proposed sheet pile design effectively mitigates the disadvantages associated with conventional pile dimensions, offering a more efficient and practical solution. Based on these considerations, the dimensions of the UHPC sheet piles selected in this study are:

- Length of fabrication of experimental piles: 6000 mm
- Width of horizontal section: 500 mm
- Horizontal section height: 250 mm
- Horizontal section thickness: 30 mm
- Arrangement of 14ϕ12 type CB400V bars, as depicted in Figure 5.
- Cross-sectional characteristics: Area A = 242 cm^2; Moment of inertia I = 17725 cm^4; Elastic bending module M_{el} = 1195 cm^3.

3) Prediction of Bearing Capacity

The bearing capacity (Bending Moment) of piles can be divided into 3 stages:

- Stage I: When the entire UHPC section is elastic (the bottom grain of the section reaches R_{bt}), as shown in Figure 6(a), at this instance, the deformation in the tensile region is still small, and the rebar steel is almost not working yet. The neutral axis at this stage is the elastic neutral axis (E. N. A.). The bearing capacity is calculated using:

$$M_{el} = W_{el}R_{bt} = 1195 \times 12 \times 10^{-4} = 1.43\ Tm \quad (1)$$

- Stage II: When half of the section height reaches *Rbt*, as portrayed in Figure 6(b), and the first cracks begin to appear. The deformation in the tensile region is still small, and the rebar steel does not work yet. The neutral axis at this stage is the plastic neutral axis (P. N. A.). The total force due to tensile stress in concrete is given by:

$$F_{bt} = \frac{A}{2} \times R_{bt} = \frac{242}{2} \times 12 \times 10^{-2} = 18.15\ T \quad (2)$$

The distance from F_{bt} to the center of the compression zone is denoted by *e,* and e = 3/4h = 18.75 cm. The moment at first crack can be calculated using:

$$M_{\text{first crack}} = F_{bt} \times e$$
$$= 18.15 \times 18.75 \times 10^{-2} = 3.4\ Tm \quad (3)$$

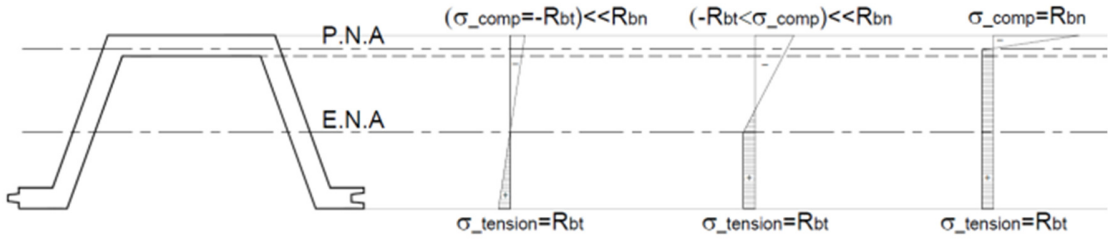

Fig. 6. Stress in the section of UHPC sheet pile.

- Stage 3: As the load continues to increase, the concrete begins to crack from the tensile zone, and the deformation gradually increases. The rebar steel begins to work, and the compression stress zone in the concrete gradually increases until it reaches R_{bn} over the thickness, which is enough to balance the amount of rebar steel. This is the extreme point of the beam, as demonstrated in Figure 6(c). The total force due to tensile stress in the bottom rebars of the tensile region is calculated using:

$$F_s = A_s R_s = 6.78 \times 350 \times 10^2 = 23.75\ T \quad (4)$$

The distance from F_s to the center of the compression zone is d, and it is nearly equal to h-a = 25-3 = 22 cm.

The bending moment is then equal to $M_{first\ crack}$ plus moment M_s created by F_s as given by:

$$M_s = F_s d = 23.75 \times 22 \times 10^{-2} = 5.23\ Tm$$

$$M = M_{first\ crack} + M_s = 3.4 + 5.23 = 8.63\ Tm \quad (5)$$

4) Load Test Scheme

The pile is subjected to a simple 4-point beam bending test in accordance with the Japanese Standard (JIS-A5373, 2004) [25], as presented in Figure 7. The experimental setup consists of a 6000 mm long fabricated beam and strain sensors, as displayed in Figures 8 and 9, respectively.

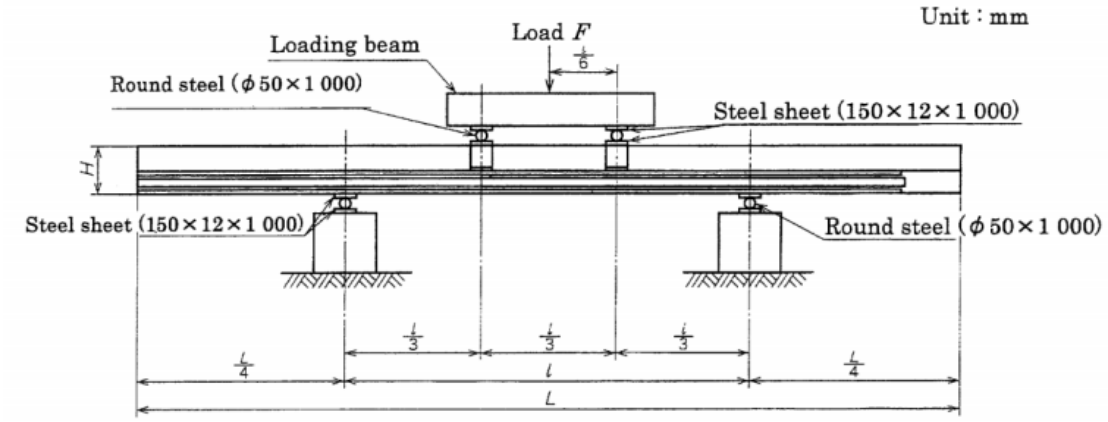

Fig. 7. Bending strength test of sheet pile (SW).

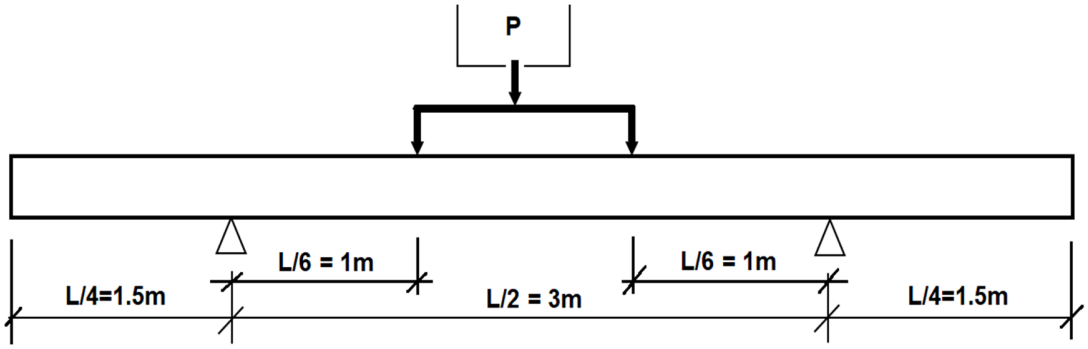

Fig. 8. Schematic diagram of the sheet pile bending test (SW).

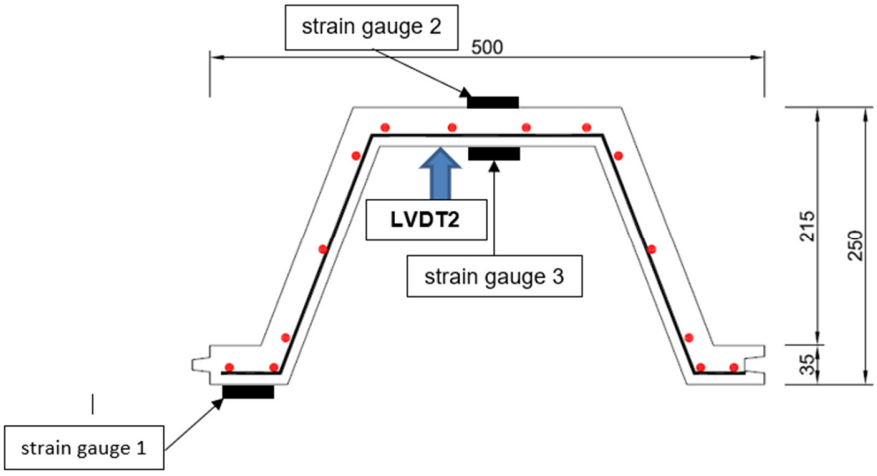

Fig. 9. Experimental setup and position of strain sensors.

The sheet pile specimens were tested under a simply supported beam configuration, with two supports and a centrally applied load. The load P, applied via a hydraulic jack, was distributed into two equal forces ($P/2$) applied symmetrically on the specimen. The total length (L) of the sheet pile sample was 6000 mm, while the experimental span length (l) was 3000 mm.

The testing was conducted as follows:

- Load application: A hydraulic jack system was used to apply the load to the specimen. The applied load was precisely measured using an electronic load cell.
- Strain measurement: The deformations in both the tension and compression zones were monitored using three resistive strain gauges (denoted as S1, S2, and S3), positioned at the mid-span section, as illustrated in Figure 9. Notably, with $L/6$ = 1 m, the bending moment at the mid-span can be calculated using the simplified formula $M = P/2$.
- Deflection measurement: Deflection was recorded using three Linear Variable Displacement Transducers (LVDTs). One LVDT (I_2) was placed at the mid-span of the beam to capture the maximum deflection, while the other two LVDTs (I_1 and I_3) were placed at the supports to monitor the boundary conditions and any potential rotation or settlement.

The maximum mid-span deflection (f) of the sheet pile specimen was determined using (6), which correlates the measured displacements to the applied loading conditions:

$$f = I_2 - \frac{(I_1+I_3)}{2} \quad (6)$$

5) Prediction of Elastic Deflection

At the end of the elastic phase (Stage I), the elastic moment reaches M_{el} = 1.43 ton-m. The equivalent load (P) at the jack is 2.86 tons. The elastic deflection of the beam was calculated using:

$$(\Delta)_{el} = \frac{23}{12} \times \frac{P\left(\frac{L}{6}\right)^3}{EI} =$$

$$\frac{23}{12} \times \frac{2.86 \times \left(\frac{6}{6}\right)^3}{48 \times 17725} \times 10^5 = 0.64\ cm \quad (7)$$

When the first crack appears, due to the presence of dispersed fibers and the high tensile strength of UHPC, the cross-section can continue to work elastically, and the deflection is calculated using (8), following the same procedure adopted in Stage I:

$$(\Delta)_{\text{first crack}} = \frac{M_{\text{first crack}}}{M_{el}} \times (\Delta)_{el} =$$

$$\frac{4.3}{1.43} \times 0.64 = 1.92\ cm \quad (8)$$

B. Fabrication and Testing of UHPC Sheet Piles

Based on the geometrical dimensions of the pile cross-section and the expected concrete pressure during casting, steel formwork was employed to manufacture the sheet piles employing a top-down pouring method. The fabrication process was meticulously planned, including detailed calculations and drawings for each pile type, which incorporated both ordinary and high-strength steel reinforcement.

The entire production sequence, comprising formwork preparation, concrete casting, curing, formwork removal, and specimen testing, was carefully executed to ensure dimensional accuracy and structural integrity. The formwork was required to meet stringent tolerances to achieve the designed geometry of the piles. Prior to concrete placement, the formwork was thoroughly cleaned, sealed, and stabilized to prevent leakage and ensure proper casting. Additionally, the interior surfaces were treated with a release agent (non-stick oil) to facilitate demolding, as illustrated in Figure 10.

(a) (b)

Fig. 10. Fabrication of sheet pile: (a) formwork oiling, (b) UHPC sheet pile.

Fig. 11. Bending test of UHPC sheet pile.

Following formwork preparation, steel reinforcement was installed according to the design specifications. Once reinforcement was in place and formwork fully assembled, the concrete casting commenced. The UHPC mixture was proportioned according to the predetermined mix design and mixed in a forced-action mixer for 15–18 min, as depicted in Figure 3. After mixing, the fresh concrete was tested for workability and then introduced into the formwork. To ensure proper consolidation and minimize voids, a vibrating table with an appropriate frequency was employed during casting. Care was taken throughout the process to avoid any impacts or disturbances that could lead to mold deformation or misalignment of reinforcement. After casting, the molds were

transferred to the curing area, where the surface was covered to maintain moisture. The concrete was cured for 24 h, after which the formwork was removed, and the specimens were prepared for subsequent testing.

IV. RESULTS AND DISCUSSION

A. Analysis of the Relationship Between Load-Deflection and Stress-Strain of Piles

1) Load–Deformation Relationship

The load-deflection relationship is presented in Figure 12, with the moment calculated according to the expression, $M = P/2$. As observed, the majority of the predicted load and moment values showed good agreement with the experimental results. However, the measured deflection was found to be 2.0-2.6 times greater than the calculated values. This discrepancy indicates that the elastic modulus (E) of UHPC in the elastic stage may not have been accurately determined, and furthermore, this parameter is not constant prior to the formation of the first crack.

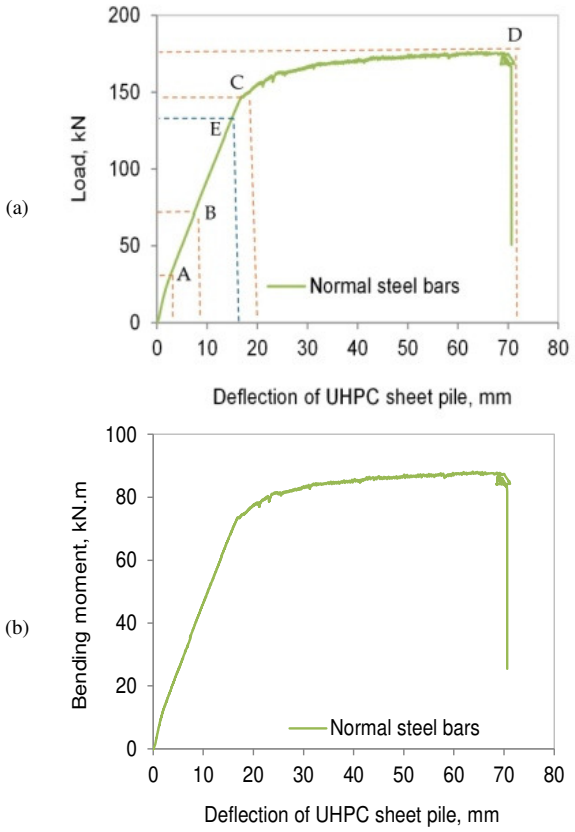

Fig. 12. (a) Load-deflection curve of UHPC sheet pile samples, (b) moment-deflection curve of UHPC sheet pile samples.

At the onset of cracking, the load reached 70.2 kN, corresponding to a deflection of 7.4 mm. Beyond this point, the specimen continued to sustain increasing loads until failure occurred at a maximum load of 176.4 kN, which is approximately 4.41 times higher than the load at first cracking. In contrast to conventional concrete, which typically fails rapidly upon reaching its limit state, the UHPC specimens exhibited a progressive failure mechanism. After cracking, the structure retained its load-bearing capacity and resisted further loading up to a large displacement of 68.4 mm before ultimate failure. This ductile behavior can be attributed to the presence of steel fibers in UHPC, which bridge cracks and dissipate destructive energy across multiple crack sites. As a result, the failure process occurred gradually, allowing for significant deformation before collapse.

TABLE V. TEST RESULTS OF UHPC SHEET PILE SAMPLES

		Point (A) elastic	**Point (B) first crack**	**Point (C) critical cracking**	**Point (D) ultimate**
Load P (kN)	Experiment	28.8	70.2	146.3	176.4
	Calculations	28.6	68.0	N/A	172.6
Deflection Δ (mm)	Experiment	3.10	7.40	17.2	68.40
	Calculations	6.40	19.2	N/A	N/A
Moment M (kN.m)	Experiment	14.4	35.1	73.2	88.20
	Calculations	14.3	34.0	N/A	86.30

Moreover, if the deflection limit is considered as $l/200 = 15$ mm, the corresponding applied load is approximately 130 kN with an associated bending moment of 6.5 MPa, representing about 75% of the ultimate load capacity. This indicates that even within serviceability limits, UHPC sheet piles maintain a substantial portion of their maximum strength, highlighting their potential for safe and reliable structural applications.

2) Stress-Strain Relationship of UHPC Sheet Piles

Figures 13(a) and (b) illustrate the stress-strain relationship for UHPC sheet piles and the tensile stress–strain response of UHPC for a commercially available UHPC containing 2% steel fiber reinforcement by volume [24, 25]. The stress in the lower fiber of the bottom flange, as monitored by sensor S1, consistently remained in tension throughout the loading process. During the elastic stage, the tensile stress in the concrete increased linearly up to approximately 12 MPa, accompanied by a relatively small strain of about 0.0015 (0.15%), indicating elastic behavior. Beyond this point, as the strain increased, the embedded steel fibers became active and began to contribute significantly to the tensile capacity.

Consequently, the stress in the concrete continued to rise, albeit at a reduced modulus of elasticity, until the strain reached approximately 0.003 (0.3%). This stress-strain relationship is consistent with the findings reported in the literature, which also highlights the transition from elastic behavior to strain-hardening due to fiber bridging mechanisms. The stress in the upper fiber of the top flange is always in a compressive state (sensor S2) with a limit deformation of about 0.0035 (0.35%). The stress in the lower fiber of the top flange is first in compression and the in-tension state (sensor S3).

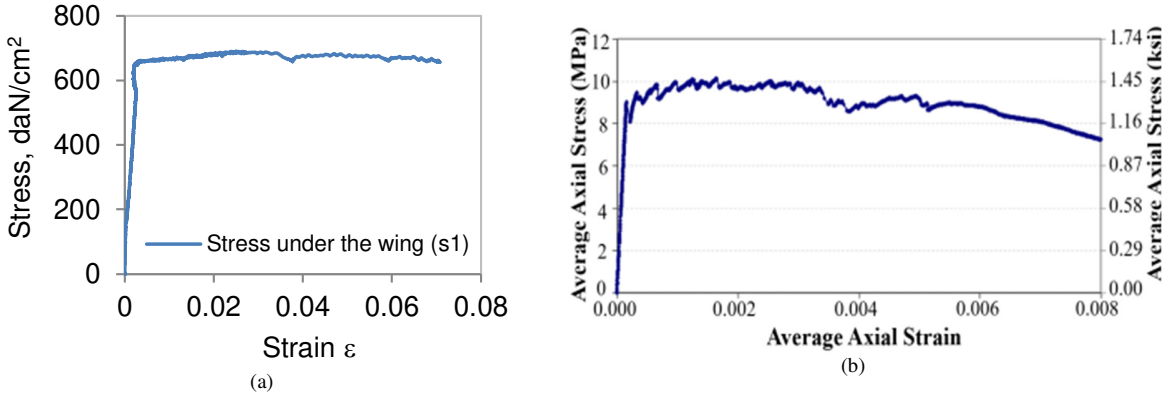

(a) (b)

Fig. 13. (a) Stress–strain relationship of the lower fiber of the bottom flange measured by S1, (b) tensile stress–strain response of a commercially available UHPC.

TABLE VI. BENDING MOMENT OF PC SHEET PILE (JIS-A5373, 2004) [25]

Type	H	T	B	S	U	Length, L (m)																
						3.0	3.5	4	4.5	5.0	5.5	6.0	6.5	7.0	7.5	8.0	8.5	9.0	9.5	10	11	12	…	21
SW120	120	60	996	15	30	O	O	O	O	O	O	O	O	O										
SW160	160	80		20	40			O	O	O	O	O	O	O	O	O								
SW180	180	80		31	62			O	O	O	O	O	O	O	O	O								
SW225	225	100		42	84					O	O	O	O	O	O	O	O	O						
SW250	250	100		55	110							O	O	O	O	O	O	O	O	O				
SW275	275	100		73	146									O	O	O	O	O	O	O	O			
SW300	300	110		94	188									O	O	O	O	O	O	O	O			
SW325A	325	110		120	240										O	O	O	O	O	O	O			
SW325B	325	110		260	260										O	O	O	O	O	O	O			

H = Height (mm), *T* = Thickness (mm), *B* = Width of Product (mm), *S* = Critical crack width strength (kN.m), *U* = Ultimate flexural strength (kN.m)

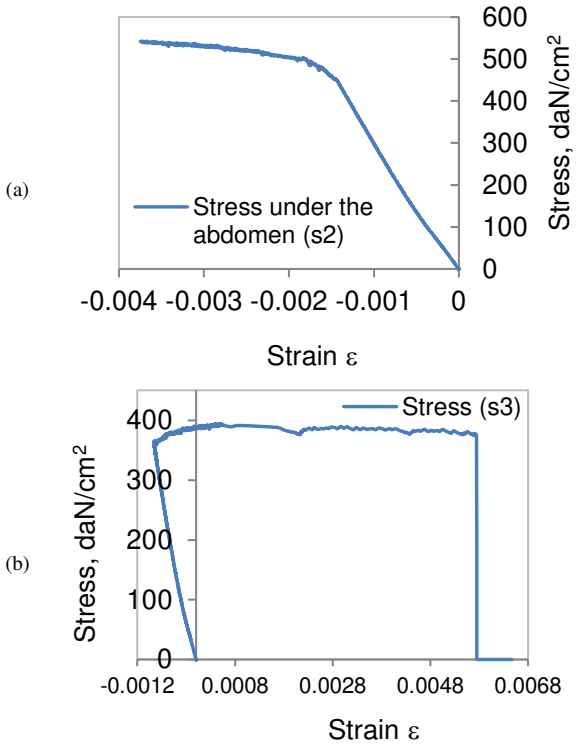

(a)

(b)

Fig. 14. (a) Stress-strain relationship for upper fiber of the top flange measured by S2, (b) stress-strain relationship for lower fiber of the top flange measured by S3.

B. Evaluation of Design Results

Based on the analysis of different theories and calculation methods, and the verification through the experimental results on the UHPC sheet pile specimens, the following evaluations can be made:

- The calculation theory for UHPC is much different from conventional RC, especially in terms of the behavior after cracking, as well as the maximum bearing capacity after the cracking of the structure.
- The theoretical calculation results with/for the sheet pile samples show that the experimental results are different for the same geometric dimensions due to the different types and content of the steel bars.

The results indicate that the load-bearing capacity at the point of the first cracking corresponds to approximately 40% of the ultimate load. The incorporation of steel fibers within the UHPC matrix significantly enhances the material's ductility, enabling the structure to maintain its load-bearing capacity even after deflections exceed the conventional serviceability limit (typically *l*/200 for normal concrete). As deflection increases beyond this limit, the steel fibers become increasingly engaged, acting as bridging elements across cracks and effectively "stitching" the fractured concrete substrate. This fiber-bridging mechanism delays the progression of cracking and prevents immediate structural failure. Failure ultimately occurs through either fiber rupture or fiber pull-out (stripping). However, given the high tensile strength of steel fibers, failure

is generally governed by fiber pull-out rather than breakage. As a result, the load-bearing capacity at failure remains significantly higher than the load associated with the allowable deflection limit, demonstrating the superior post-cracking performance and energy dissipation capability of UHPC-reinforced sheet piles.

From the results of theoretical and experimental analysis, it is shown that UHPC sheet piles with high bearing capacity can completely replace PC sheet piles in special cases, such as in corrosive environments, where it is necessary to keep determining the construction wall. In fact, the bending moments at the critical cracking state and the ultimate state of the PC sheet pile, as presented in Table VI, (with the same height but twice the thickness) are 55 kN·m (compared to 146.4 kN·m for the UHPC sheet pile) and 110 kN·m (compared to 176.4 kN·m for the UHPC sheet pile), respectively.

In addition, in terms of execution, UHPC sheet piles possess lightweight and small wall thickness; thus, the construction process is as easy as that of steel Larsen sheet piles.

V. CONCLUSIONS

Based on the findings of the presentresearch, the following conclusions are drawn:

- The design and calculation approach for Ultra-High-Performance Concrete (UHPC) differs significantly from that of conventional reinforced concrete, particularly regarding the post-cracking behavior and ultimate load-bearing capacity. Utilizing the superior mechanical properties of UHPC, this study successfully designed sheet pile elements with a height of 250 mm, a width of 500 mm, and a wall thickness of 30 mm, reinforced with steel bars.
- The experimental results confirmed that UHPC sheet piles reinforced with steel bars fully meet the targeted performance objectives. Specifically, they exhibited higher bending moments than conventional RC piles of the same dimensions, with excellent agreement between the theoretical predictions and experimental outcomes. Notably, the load-bearing capacity at the first crack was approximately 40% of the ultimate capacity.
- The UHPC sheet piles demonstrated adequate load-bearing performance to satisfy the design requirements, especially in applications requiring resistance to aggressive environmental conditions. Furthermore, due to their reduced wall thickness and lighter weight, UHPC sheet piles offer significant advantages in terms of ease of transportation and installation. These characteristics make them particularly suitable for use as retaining walls in corrosive environments and in situations where permanent fixation is required.

Overall, the results highlight UHPC as a highly promising material for next-generation sheet pile systems, offering a sustainable, durable, and cost-effective alternative for infrastructure in aggressive and space-constrained environments, while paving the way for further research and wider practical implementation.

REFERENCES

[1] A. Hettler and K. Kurrer, *Earth Pressure*, 1st ed. Hoboken, NJ, USA: Wiley, 2019.

[2] G. Jürgen, *Sheet Piling Handbook*, 3rd ed. Hamburg, Germany: ThyssenKrupp Bautechnik GmbH, 2008.

[3] J. Morley, D. Waite, and J. E. O'brien, *Steel Sheet Piling in Coast-Protection Works, Shoreline Protection*. London, UK: Thomas Telford Ltd, 1983.

[4] P. Richard and M. Cheyrezy, "Composition of Reactive Powder Concretes," *Cement and Concrete Research*, vol. 25, no. 7, pp. 1501–1511, Oct. 1995, https://doi.org/10.1016/0008-8846(95)00144-2.

[5] M. B. Eide and J. M. Hisdal, "Ultra High Performance Fibre Reinforced Concrete (UHPFRC) – State of the art," SINTEF Building and Infrastructure, Trondheim, Norway, Project Report PR-44-2012, 2012.

[6] *Standard Practice for Fabricating and Testing Specimens of Ultra-High Performance Concrete*, ASTM C1856-17, ASTM International, West Conshohocken, PA, USA, 2017.

[7] "Ultra-High-Performance Concrete: An Emerging Technology Report," American Concrete Institute, Farmington Hills, MI, USA, Technical Report ACI 239R-18, Oct. 2018.

[8] P. Richard and M. H. Cheyrezy, "Reactive Powder Concretes With High Ductility and 200 - 800 Mpa Compressive Strength," in *SP-144: Concrete Technology: Past, Present, and Future*, American Concrete Institute, 1994, pp. 507–518.

[9] M. Schmidt and E. Fehling, "Ultra-High-Performance Concrete: Research, Development and Application in Europe," *ACI Special Publication*, vol. 228, Jan. 2005.

[10] M. Odelola, S. S. K. Dolati, A. Mehrabi, and D. Garber, "Ultra-High-Performance Concrete (UHPC) Piles and Splicing Options," *Applied Sciences*, vol. 14, no. 2, Jan. 2024, Art. no. 827, https://doi.org/10.3390/app14020827.

[11] J. Su, Z. Su, W.-T. Wu, B.-C. Chen, and T. Deng, "Experimental and Numerical Studies on Strong-Axis and Weak-Axis Bending Performance of H-Shaped Prestressed UHPC Members," *Structures*, vol. 74, Apr. 2025, Art. no. 108495, https://doi.org/10.1016/j.istruc.2025.108495.

[12] Y. Zhang, H. Zheng, and G. Li, "Experimental Study of UHPC-RC Composite Pile Connected by Shear Keys," *Structural Engineering International*, vol. 32, no. 2, pp. 189–202, Apr. 2022, https://doi.org/10.1080/10168664.2021.2010633.

[13] H. D. Nguyen, S. Khatir, and Q. B. Nguyen, "A Novel Method for the Estimation of the Elastic Modulus of Ultra-High Performance Concrete using Vibration Data," *Engineering, Technology & Applied Science Research*, vol. 14, no. 4, pp. 15447–15453, Aug. 2024, https://doi.org/10.48084/etasr.7859.

[14] H. Yazıcı, M. Y. Yardımcı, H. Yiğiter, S. Aydın, and S. Türkel, "Mechanical Properties of Reactive Powder Concrete Containing High Volumes of Ground Granulated Blast Furnace Slag," *Cement and Concrete Composites*, vol. 32, no. 8, pp. 639–648, Sep. 2010, https://doi.org/10.1016/j.cemconcomp.2010.07.005.

[15] Q.-M. Phan, V.-P. Nguyen, T.-N. Hoang, and N.-T. Vu, "A Novel Approach using Sustainable Structures in Preventing Coastal Erosion and Forming Sandy Beach in Vietnam," *IOP Conference Series: Materials Science and Engineering*, vol. 869, no. 7, Jun. 2020, Art. no. 072053, https://doi.org/10.1088/1757-899X/869/7/072053.

[16] J. Li, C. Wu, H. Hao, Z. Wang, and Y. Su, "Experimental Investigation of Ultra-High Performance Concrete Slabs under Contact Explosions," *International Journal of Impact Engineering*, vol. 93, pp. 62–75, Jul. 2016, https://doi.org/10.1016/j.ijimpeng.2016.02.007.

[17] M. Rafieizonooz, J.-H. J. Kim, J.-S. Kim, and J.-B. Jo, "Effect of Carbon Nanotubes on Chloride Diffusion, Strength, and Microstructure of Ultra-High Performance Concrete," *Materials*, vol. 17, no. 12, Jun. 2024, Art. no. 2851, https://doi.org/10.3390/ma17122851.

[18] H. T. Nghia, "Experimental Study to Produce Manhole Cover Using Ultra-High Performance Concrete," *International Journal of GEOMATE*, vol. 21, no. 85, Sep. 2021, https://doi.org/10.21660/2021.85.j2244.

[19] F. De Larrard and T. Sedran, "Optimization of Ultra-High-Performance Concrete by the use of A Packing Model," *Cement and Concrete Research*, vol. 24, no. 6, pp. 997–1009, 1994, https://doi.org/10.1016/0008-8846(94)90022-1.

[20] F. De Larrard, *Concrete Mixture Proportioning: A scientific approach*. London, UK: CRC Press, 1999.

[21] M. R. Jones, L. Zheng, and M. D. Newlands, "Comparison of Particle Packing Models for Proportioning Concrete Constituents for Minimum Voids Ratio," *Materials and Structures*, vol. 35, no. 5, pp. 301–309, Jun. 2002, https://doi.org/10.1007/BF02482136.

[22] *Standard Test Method for Compressive Strength of Cylindrical Concrete Specimens*, ASTM C39/C39M-21, ASTM International, West Conshohocken, PA, USA, 2021.

[23] *Test Method for Flexural Performance of Fiber-Reinforced Concrete (Using Beam With Third-Point Loading)*, ASTM C1609/C1609M-19a, ASTM International, West Conshohocken, PA, USA, 2019.

[24] *Standard Test Method for Static Modulus of Elasticity and Poisson's Ratio of Concrete in Compression*, ASTM C469/C469M-14, ASTM International, West Conshohocken, PA, USA, 2014.

[25] *Precast Prestressed Concrete Products*, JISA5373, Japanese Standards Association, Tokyo, Japan, 2016.